This is accepted version of this manuscript. After copy editing and type setting, it will appear in Paleoceanography and Paleoclimatology, *doi 10.1029/2021PA004400*

Elevated Post K-Pg Export Productivity in the Gulf of Mexico and Caribbean

Christopher M. Lowery[1]*, Timothy J. Bralower[2]

[1]University of Texas Institute for Geophysics, Austin, TX

[2]Pennsylvania State University, University Park, PA

*corresponding author: cmlowery@utexas.edu

Key Points

Main point #1: Post K-Pg export productivity was elevated across the Caribbean-Gulf of Mexico region for ~ 300 kyr

Main point #2: At sites with a clearly defined micrite layer, the end of micrite deposition coincides with the top of the highest productivity interval

Main point #3: Elevated post K-Pg export productivity appears to be a feature of oligotrophic low latitude open ocean sites

Abstract

The global heterogeneity in export productivity after the Cretaceous-Paleogene (K-Pg) mass extinction is well documented, with some sites showing no change on geologic timescales, some demonstrating sustained decline, and a few showing a somewhat surprising increase. However, observational data come from sites so widespread that a key outstanding question is the geographic scale of changes in export productivity, and whether similar environments (e.g., open ocean gyres) responded similarly or whether heterogeneity is unrelated to environment. To address this, we developed three new Ba/Ti export productivity records from sites in the Gulf of Mexico and Caribbean which, combined with

published data from a fourth site in the Chicxulub Crater itself, allow us to reconstruct regional changes in post K-Pg export productivity for the first time. We find that, on a regional scale, export productivity change was homogenous, with all four sites showing a ~300 kyr period of elevated export production just after the boundary, followed by a longer period of decline. Interestingly, this interval of elevated export production appears to coincide with the post K-Pg global micrite layer, which is thought to at least partially have been produced by blooms of carbonate-producing cyanobacteria and other picophytoplankton. Global comparison of sites shows that elevated export productivity appears to have been most common in oligotrophic gyres, which suggests that changing plankton ecology evidenced by the micrite layer altered the biological pump, leading to a temporary increase in export production in these settings.

Plain Language Summary

Primary producers are the base of the food chain; this group was severely damaged by the environmental effects associated with the Cretaceous-Paleogene mass extinction. Determining how primary production recovered after this calamity is an important foundation for understanding how ecosystems recovered. Most previous work has focused on a process called export production, whereby organic carbon produced by phytoplankton is transferred to the ocean interior (some of which sinks to the seafloor and is buried). This work has shown that although most parts of the ocean recorded a decline in export production after the extinction event, some regions actually showed an increase. However, it was not clear on what geographic scale these differences occurred, or what caused them. We generated three new records of export production from a single region, the Gulf of Mexico/Caribbean Sea, and found a consistent increase in export production at each site for the same period of time after the extinction event. Comparison with other sites with increased export production shows that many are from open ocean gyres, suggesting that these regions were predisposed to increased export production in the earliest Paleocene because they were characterized by low productivity prior to the extinction.

1. Introduction

The end Cretaceous mass extinction was associated with a severe disruption of marine productivity (Hsü and Mackenzie, 1985; Zachos et al., 1989; D'Hondt et al., 1998; Coxall et al., 2006; Birch et al., 2016). A reduction in sunlight received at Earth's surface caused by dust, soot, and sulfate aerosols ejected by the Chicxulub impact resulted in a reduction in photosynthesis which is thought to have led to the collapse of marine food webs (Alvarez et al., 1980; D'Hondt et al 1998). Models show that the reduction in insolation lasted only a few years after the impact (Toon et al., 1997; Brugger et al., 2017; Artemieva et al., 2017; Bardeen et al., 2017; Artemieva and Morgan, 2020; Alegret et al., 2022), removing the proximal external stress on marine primary producers and clearing the way for the recovery of primary production. How, exactly, marine productivity recovered has been a focus of K-Pg boundary research for decades; the K-Pg mass extinction represents a geologically unique disruption of marine ecosystems, perhaps the only major event in Earth history which happened faster than modern climate change and environmental disruption. Modern oceans are likely on the verge of a major reorganization of dominant plankton types due to warming, acidification, and changes in circulation and ventilation patterns (e.g., Barton et al., 2016; Jonkers et al., 2019), and primary production is expected to decline 20% due to warming (Moore et al., 2018). The earliest Paleocene provides a window into understanding how such ecological changes may impact food webs and marine carbon burial.

Of course, we can't observe ancient primary production in the euphotic zone directly, so most work on the collapse and recovery of productivity after the K-Pg boundary has focused on sedimentary records of export production (the transfer of particulate organic matter from the euphotic zone to the deep sea; e.g., Passow and Carlson, 2012)). The movement of particulate organic matter (POM) from the euphotic zone to the seafloor is complicated and can be divided into a series of steps, all of which are influenced by different processes. Most net primary production (NPP) occurs in the euphotic zone (dependent on sunlight penetration but typically defined as 0-100 or 200 m water depth; Passow and Carlson, 2012), and most POM is remineralized in these near surface waters. The precise amount varies by region and season, but typically ~ 90% of NPP is consumed and recycled before it can sink out of the

euphotic zone. The movement of POM out of the euphotic zone is what biological oceanographers define as "export flux" or "export productivity" (Passow and Carlson, 2012). Paleoceanographers typically use the latter term to refer to the whole process by which POM is buried in the sediments. However, here we follow the biological oceanographers and use "export productivity" to refer to this initial sinking out of surface waters, mainly because this is the process that can be tracked in ancient sediments by biogenic barium concentration – see below). As POM continues sinking through the mesopelagic zone (typically defined as 100-1000 m water depth; Passow and Carlson, 2012) it is subject to grazing by mesopelagic organisms of all sizes, which gradually break down long chain organic carbon molecules to their constituent inorganic carbon molecules, turning POM into dissolved organic carbon (DOC) and then dissolved inorganic carbon (DIC) (e.g., Boyd and Trull, 2007). The amount of remineralization in the mesopelagic zone is controlled by the rate at which the POM is sinking (i.e., how long it is exposed to mesopelagic grazers), the composition of the grazing ecosystem, and the quality of the organic carbon (i.e., is it labile and easy to degrade or refractory and more difficult to break down) (e.g., Buessler and Boyd, 2009; Henson et al., 2012). POM which sinks below the mesopelagic zone is effectively removed from the short-term carbon cycle, and so the export of organic matter below 1000 m is often referred to as "sequestration flux" (e.g., Passow and Carlson, 2012) or "transfer efficiency" (Henson et al., 2012). By this point, most remineralization has occurred, but POM sinking out of the mesopelagic zone has traveled through less than one third of the average depth of the ocean, and additional remineralization occurs all the way to (and at) the seafloor, before surviving POM is buried and removed from the carbon cycle on geologic time scales (referred to as "burial flux" by Griffith et al., 2021). The amount of net primary production that reaches the deep sea varies by region and is largely controlled by plankton ecology (Henson et al., 2012), but on the whole only 1-3% of modern net primary production reaches the deep ocean or sediments (e.g., Müller and Suess, 1979; de la Rocha and Passow, 2007; Griffith et al., 2021).

Initial reconstructions of productivity change across the K-Pg boundary focused on carbonate proxies, specifically carbonate mass accumulation rates and carbon stable isotopes (e.g., Hsü and

99 Mackenzie, 1985; Zachos et al., 1989). A drop in carbonate mass accumulation rate in the deep sea has
100 been observed at many boundary sites across the globe, and is interpreted to represent a reduction in the
101 production of carbonate by pelagic calcifiers like calcareous nannoplankton and planktic foraminifera
102 (e.g., D'Hondt et al., 1998), both of which suffered severe (>90% species diversity) extinction at the K-Pg
103 boundary (e.g., Thierstein, 1982; Bown, 2005; Fraass et al., 2015; Lowery et al., 2020). The most striking
104 carbonate proxy response, though, is the collapse of the $\delta^{13}C$ gradient between the surface ocean and the
105 deep sea (Zachos and Arthur, 1986; Zachos et al., 1989; D'Hondt et al., 1998; Coxall et al., 2006; Alegret
106 et al., 2012; Esmeray-Senlet, 2015; Birch et al., 2016). In the modern ocean (and likely since
107 phytoplankton first evolved) the sinking of ^{12}C-rich organic matter depletes the surface ocean and
108 enriches the seafloor in that light isotope, resulting in an isotopic gradient from surface to seafloor. This
109 gradient collapsed at the Cretaceous-Paleogene (K-Pg) boundary (e.g., Hsü et al., 1982; Kump, 1991),
110 reflecting a reduction in export production and a weakening of the biological pump for 1.8 myr (Birch et
111 al., 2016, 2021). Taking into account observed changes in planktic foraminifer ecology and physiology
112 (which account for a portion of the change in the $\delta^{13}C$ gradient – Birch et al., 2016, 2021), modelling
113 suggests that a ~50% decrease in the amount of organic carbon exported from the euphotic zone, from
114 10% of net primary production to 5%, would account for the observed collapse of the $\delta^{13}C$ gradient
115 (D'Hondt et al., 1998; Henehan et al., 2019).

116 The continued flux of some organic matter to the deep ocean is confirmed by fossil data which
117 indicate a lack of extinction in some groups of pelagic fishes (Doyle, 1979; Siebert and Norris, 2015) and
118 deep sea benthic foraminifera (e.g., Thomas, 1990; Culver, 2003; Alegret and Thomas, 2005, 2007, 2009;
119 Alegret et al., 2012, 2021). Meanwhile, geochemical data indicate a rapid recovery of primary producers
120 (Sepúlveda et al., 2009, 2019). One of the most striking features of the benthic foraminiferal record at the
121 K-Pg boundary is its global variability. Although no major extinction occurred, assemblage compositions
122 shifted at many sites (e.g., Culver et al., 2003; Alegret et al., 2012, 2021). At some localities, benthic
123 foraminifer assemblages indicate a reduction in the flux of organic matter to the seafloor, but others show

no significant change across the boundary, and some actually indicate an *increase* in organic matter flux (e.g., Alegret and Thomas 2005, 2007, 2009; Alegret et al., 2012, 2021).

In practice, it is difficult to use carbon isotope gradients to reconstruct post K-Pg export production in geographic detail. Isotopic analysis of planktic and benthic foraminifera requires well-preserved carbonate material, otherwise diagenetic overprinting will obscure the signal. Localities with well-preserved 66-myr-old foraminifera are not particularly common, and thus carbon isotope gradients have only been produced from a handful of well-studied sites like Walvis Ridge (Hsü et al., 1982; Hsü and Mackenzie, 1985; D'Hondt, 1998a; Coxall et al., 2006; Alegret et al., 2012; Birch et al., 2016, 2021), Shatsky Rise (Zachos and Arthur, 1986; Zachos et al., 1989; Coxall et al., 2006), J-Anomaly Ridge (Zachos and Arthur, 1986), and São Paulo Plateau (Zachos and Arthur, 1986). While these sites have all yielded high quality data that have fundamentally changed our understanding of K-Pg recovery, they only cover a small part of the ocean.

For this reason, additional proxies not dependent on pristine microfossil preservation are necessary. Benthic foraminifera, which track burial flux of POM, are one such proxy, and another is based on barium. Biogenic barium concentration in marine sediments (where it is commonly preserved as barite – $BaSO_4$) has been shown to correlate with export production in the modern and ancient ocean (Dymond et al., 1992; Francois et al., 1995; Eagle et al., 2003; Paytan and Griffith, 2007) and is not subject to the same diagenetic effects as carbon isotopes. Like so many other proxies, though, studies have shown that the relationship between the measurement (biogenic barium) and the thing for which it is a proxy (export production) is not quite straight forward. Carter et al. (2020) provide a good review of the processes which can affect the formation, burial, and preservation of marine barite. Here we summarize the most important processes that impact the reconstruction of changes in export production across the K/Pg boundary.

Although marine barite is linked to export production, Ba can also be sourced from detrital settings, and the Ba content can vary from source area to source area (e.g., Carter et al., 2020), so

elemental Ba data need to be normalized against a terrigenous element like titanium or aluminum to control for any possible detrital barium component (e.g., Dymond et al., 1992; Payton et al., 1996; Bains et al., 2000; Paytan and Griffith, 2007; Griffith and Paytan, 2012). Most marine barite formation occurs between 200-600 m water depth, where most organic matter remineralization occurs (Martinez Ruiz et al., 2020; Carter et al., 2020), and so biogenic Ba production tracks "export flux" or the amount of POM which sinks below the euphotic zone (see above). However, Ba formation is probably mediated by bacteria which consume oxygen during remineralization of POM, which means that increased bacterial production could lead to increased barite formation (e.g., Dehairs et al., 2008; Jacquet et al., 2011; Planchon et al., 2013) without a change in export production. This microbial activity can be influenced by organic matter quality, temperature (as warmer temperatures result in increased bacterial metabolic rates), and the composition of the microbial ecosystem itself (Carter et al., 2020). Ba *production* is thus (mostly) correlated directly to the export flux of POM, but the ocean is undersaturated in barite, which means that 70% of particulate barite (and more in anoxic regions) dissolves in the water column and the upper few cm of the sediments before it is buried (Carter et al., 2020). This means that the replacement of one watermass with another of a different Ba^{2+} saturation state could lead to a change in barite accumulation which could be misinterpreted as a change in export flux (e.g., Paytan et al., 2007; Carter et al., 2020).

These caveats make it difficult to directly extrapolate from Ba flux to absolute values of export flux in mass of organic carbon per unit time, particularly all the way back in the Paleocene, but if major variables (terrigenous flux, water mass changes) are controlled for, then marine barite can provide important insights to changes in export flux. Hull and Norris (2011) used XRF-derived Ba/Ti and Ba/Fe ratios from five K-Pg boundary sites to bolster the export productivity record of benthic foraminifera, and demonstrated that changes in export production across the boundary were indeed geographically heterogeneous, with some sites showing an increase in export production after the boundary.

Understanding geographic heterogeneity in export production is necessary to understand the overall recovery of marine primary producers after the K-Pg boundary. In particular, the calcareous

nannoplankton, which have the best fossil record among primary producers in the early Paleocene, exhibit geographic heterogeneity in their post K-Pg recovery (Jiang et al., 2010; Schueth et al. 2015; Jones et al., 2019). Post-extinction calcareous nannoplankton assemblages are characterized by a dominance of "disaster taxa," chiefly *Braarudosphaera* and *Cervisiella,* which eventually give way to a succession of acme events as new Paleocene genera appear and briefly dominate the assemblage (Bown, 2005; Jones et al., 2019; Gibbs et al., 2020). Gibbs et al. (2020) found that some of the survivors and earliest new genera have adaptations which indicate a mixotrophic lifestyle (i.e., they supplemented photosynthesis by ingesting small prey like bacteria); later incoming taxa lack these adaptations, indicating changing trophic conditions (specifically the under exploitation of small prey species following the extinction of many heterotrophic plankton) may have played a role in nannoplankton recovery (Gibbs et al., 2020). The timing of these acme events is geographically variable, and at sites with elevated export productivity after the K-Pg (Shatsky Rise and Chicxulub Crater), it is coincident with an observed decline in export production (Jones et al., 2019). In the ocean today, eutrophic waters tend to be dominated by a few taxa best suited to take advantage of widely available food, while oligotrophic waters tend to have much higher diversity with greater degrees of specialization (e.g., Hallock, 1987). Jones et al. (2019) hypothesized that the recovery of primary producer assemblages (and by extension the ecosystems which they supported) after the K-Pg is similarly linked to nutrient state controlled by the recovery of the biological pump, but the linkages are not well understood and a better picture of export productivity trends is a necessary first step.

Unfortunately, geographic trends in early Paleocene export productivity are still poorly known. Modelling by Henehan et al. (2019) indicated that typically oligotrophic gyre environments in the North and South Pacific Oceans, the Arctic Ocean, and northern Indian Ocean, would have experienced increased export productivity in a scenario in which global average export productivity declined 50% (in line with estimates of post-K-Pg declines in export production; D'Hondt et al., 1998; Henehan et al., 2019). However, these modelling results are currently unconstrained by data, and sites with observed

increases in post-extinction export production (e.g., Shatsky Rise Site 1209; Hull and Norris, 2011) are close to, but fall outside of, modelled areas of increased post-extinction export production. Hull and Norris (2011) represents a significant improvement in observations of export productivity trends, but are limited to the ocean basin scale: e.g., Shatsky Rise in the North Pacific compared to São Paulo Plateau in the South Atlantic compared to Maud Rise in the Southern Ocean. This is a good starting place but leaves open the question of the scale of heterogeneity. Do regions exhibit similar trends (implying an oceanographic driver of variability) or do sites vary even within a region (implying that variability is driven by local effects or is just stochastic)? To address this question, we developed three Ba/Ti datasets from the Gulf of Mexico and Caribbean at Deep Sea Drilling Project (DSDP) Site 95 and Ocean Drilling Program (ODP) Sites 999 and 1001, which we combined with published data from International Ocean Discovery Program (IODP) Site M0077 in the Chicxulub Crater (Lowery et al., 2021) to produce the first regional-scale study (~1700 km) of export productivity after the K-Pg. This region was modelled to have been characterized by low export production in the latest Cretaceous (Henehan et al., 2019) and thus may be predicted to have exhibited increased export production after the boundary. We found that earliest Danian export productivity is elevated at all Gulf of Mexico and Caribbean sites and that an initial reduction in export production occurs ~ 300 kyr after the boundary at all sites, indicating that export productivity trends were homogeneous at a regional scale.

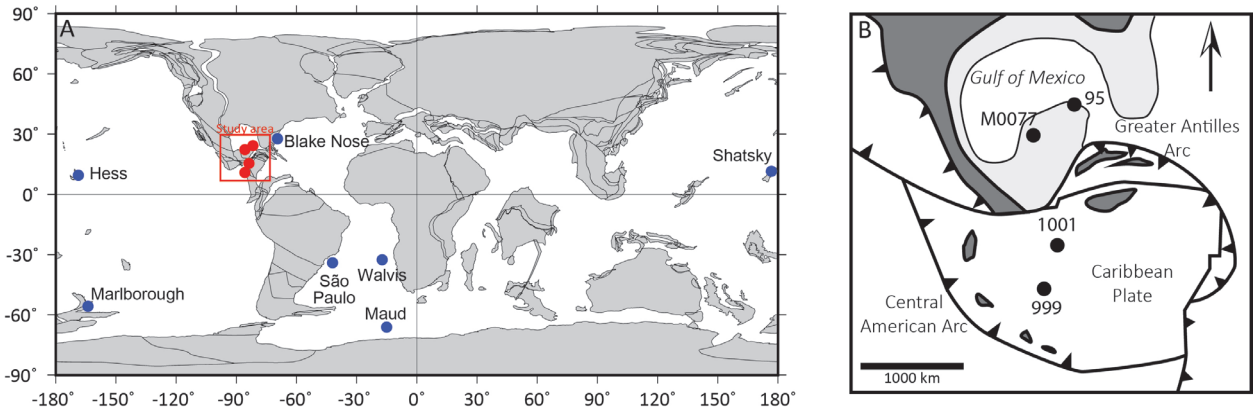

Figure 1. *A) Global plate tectonic reconstruction from 66 Ma showing location of our study area (in red) and other notable sites discussed in this paper (in orange). Grey areas are continental blocks, terranes, and plateaus; map from ODSN generated at https://www.odsn.de/odsn/services/paleomap/paleomap.html. B) Regional map showing position of our study sites around the time of the K-Pg Boundary. Map modified after Pindell and Barrett (1990) and Snedden et al. (2021). Black indicates land and grey indicates continental platforms.*

1.1 Study Sites

We looked at three scientific ocean drilling sites in the greater Caribbean region with a well-preserved K-Pg boundary interval and compared them to published XRF data from IODP Site M0077 in the Chicxulub Crater (Figure 1). An additional site, DSDP Site 536, below the Campeche Escarpment in the southeastern Gulf of Mexico (Buffler et al., 1984), was considered but rejected because a preliminary examination of planktic foraminifera in the nominally lowermost Paleocene cores found a mix of biozones ranging from the Cretaceous to the late Paleocene, indicating significant reworking and/or drilling disturbance, suggesting that XRF data would be untrustworthy. All four sites appear to have been at roughly bathyal water depths in the earliest Danian (Worzel et al., 1983; Buffler et al., 1984; Sigurdsson et al., 1997; Lowery et al., 2018). These tropical/subtropical sites are characterized by pelagic carbonate deposition throughout the study interval.

DSDP Site 95, drilled in 1970 on the northeasterly margin of the Yucatan Platform on the Campeche Escarpment (Worzel et al., 1973), contains the correct order of planktic foraminifer biozones and decent preservation in a mostly-complete section overlying the K-Pg impact layer. The Chicxulub impact (and associated earthquakes, tsunami, and seiche waves) caused widespread mass-wasting across the Gulf of Mexico, resulting in K-Pg boundary deposits 10s to 100s of m thick (e.g., Bralower et al., 1998; Denne et al., 2013; Sanford et al., 2016). Site 95, due to its perched position on the edge of the Yucatan Platform, only has ~ 3 m of reworked Cretaceous material and impact debris (Figure 2A). The top of the K-Pg boundary layer occurs at the top of Core 13. This is not the K-Pg boundary per se, because the base of the Paleocene is defined at its Global Stratotype Section and Point at El Kef, Tunisia, as the lowest occurrence of impact material which means that the Cretaceous ended at “the moment of the meteorite impact” (Molina et al., 2006). The impact layer in the Gulf of Mexico is thus technically earliest Danian in age.

Site 1001 was drilled in 1995-6 during ODP Leg 165, and is located on the Hess Escarpment on the Nicaragua Rise (Figure 1). Shipboard biostratigraphy placed the K-Pg boundary between Core 1001A-38R-CC and 1001A-39R-1 (Figure 2B). Unlike the thick K-Pg boundary deposits in the Gulf of Mexico, here the whole interval is just a few cm thick. Maastrichtian limestone is overlain by a 1 cm thick dark greenish gray clay, which is in turn overlain by a 3.5 cm bluish gray claystone containing 1 mm scale dark green spheroids interpreted to be tektites (Sigurdsson et al., 1997). This tektite layer is turn

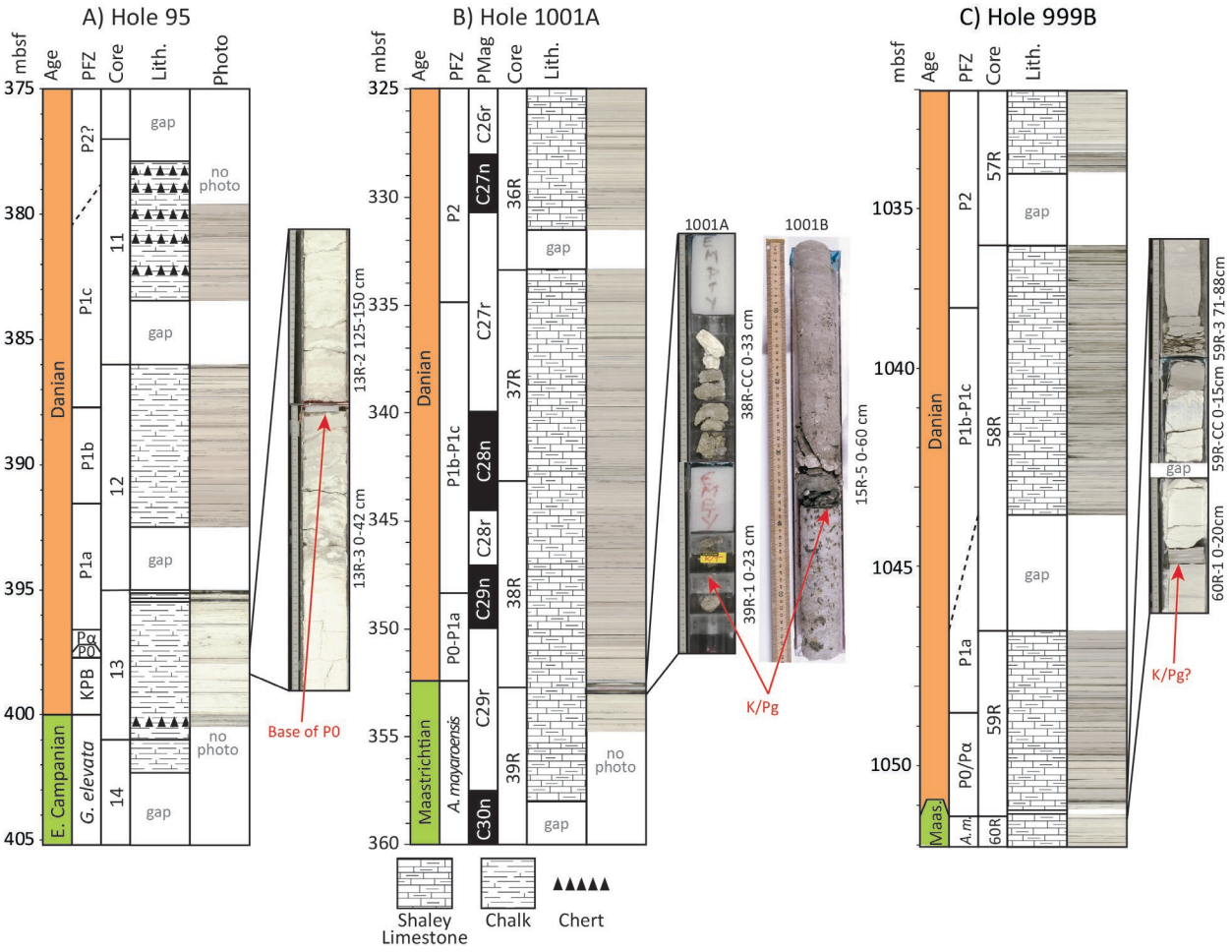

Figure 2. *Stratigraphic sections showing lithostratigraphy, core scan photographs, and images of the K-Pg boundary of the studied intervals from DSDP Hole 95, ODP Hole 1001A, and ODP Hole 999B. Lithostratigraphy follows shipboard descriptions Worzel, Bryant et al. (1973) for Site 95 and Sigurdsson et al., 1997 for Sites 999 and 1001). Core scan photographs were collected at the GCR at the same time XRF data were collected (except for the photograph of the K-Pg boundary in Hole 1001B, which is from the ODP photo archives). Mbsf = meters below sea floor, PFZ = Planktic Foraminifer Zone, Lith. = lithology, PMag = Paleomagnetic polarity, E. Campanian = Early Campanian, Maas. = Maastrichtian, G. elevata = Globotruncanita elevata, A.m. and A. mayaroensis = Abathomphalus mayaroensis.*

overlain by a 3.5 cm medium gray to greenish gray claystone which contains shocked quartz (Sigurdsson et al., 1997). The boundary sequence, identified on the basis of biostratigraphy and impact debris, is overlain by a 4 cm thick light grey limestone assigned to planktic foraminifer Biozones P0/Pα undifferentiated based on thin section analysis (the zones are undifferentiated because the biostratigraphers were not confident in their ability to identify the taxon differentiating the zones, *Parvularugoglobigerina eugubina*, in thin section; Sigurdsson et al., 1997). Shipboard biostratigraphy in the Paleocene is of poor quality due to the extremely poor preservation of fossil material in the indurated limestone. A magnetic polarity timescale was published for Site 1001 by Louvel and Galbrun (2000) based on whole core scans and single samples, as well as a downhole wireline tool called the Geological High-sensitivity Magnetic Tool (GHMT), and the resulting magnetic reversal timescale means that Site 1001 has the best age model of the sites examined here. Although Hole 1001B recovered a more complete boundary section than Hole 1001A (Figure 2B), Hole 1001B has a number of coring gaps in both the uppermost Cretaceous and the early Paleocene, so XRF scans were conducted on Hole 1001A.

Site 999 was also drilled in 1995-6 during Leg 165 and is located on Kogi Rise in the Colombian Basin (Figure 1). Shipboard biostratigraphy placed the K-Pg boundary near the boundary between Cores 999B-59R and 999B-60R (Figure 2C). The highest occurrence of common Maastrichtian calcareous nannoplankton was observed in Sample 999B-60R-1 10 cm, and that of Maastrichtian planktic foraminifera in a thin section in Sample 999B-60R-1 1-21 cm (Sigurdsson et al., 1997). The few foraminifera observed in thin section between Samples 999B-59R-CC 15cm (the base of the core catcher) and 999B-60R-1 1 cm were composed primarily of survivor species *Guembelitria cretacea* (Sigurdsson et al., 1997). The shipboard biostratigraphers were not confident that tiny trochospiral specimens observed in the same sample were or were not *P. eugubina* and thus conservatively assigned this interval to Zones P0/Pα undifferentiated (Sigurdsson et al., 1997). The bases of Zones P1a (top of *P. eugubina*), P1b (base of *Subbotina triloculinoides*), and P2 (base of *Praemurica uncinata*) were identified shipboard (Sigurdsson et al., 1997) and form the basis for the age model used here, although the latter two are of

lower confidence. We washed and examined samples from Site 999 to see if we could refine the shipboard age model but poor microfossil preservation in the indurated limestone material prevented us from adding anything new. A white indurated limestone overlies the highest Cretaceous nannoplankton observed in Core 60, and the base of Section 59R-CC contains a 1 mm thick claystone. Comparison of the recovered core and borehole images collected by the formation microscanner tool reveals that this claystone is ~ 9 cm thick in the borehole, and thus ~ 8 cm of this unit were not recovered (Sigurdsson et al., 1997). It seems reasonable to assume that this missing interval is equivalent to the 8 cm of ejecta-bearing claystones described at Site 1001. The claystone is overlain by 10 cm thick mottled blue limestone described by shipboard scientists as having the appearance of "Roquefort Blue Cheese" and assigned to planktic foraminifer Zones P0/Pα (Sigurdsson et al., 1997). This white limestone is a common feature of K-Pg boundary sections in the deep sea, and is comprised of micrite (i.e., microcrystalline calcite; Bralower et al., 2020). Although the white limestone only extends 10 cm above the boundary, Bralower et al. (2020) observed micrite at Site 999 over a total thickness of 2.42 m. A 2 m coring gap occurs at the base of Core 999B-58R in planktic foraminifer Zone P1a. Micrite was also identified at Site 1001 but it was limited to the core catcher of core 1001A-38R, which contains a few discontinuous bits of rubble and a large void space (Figure 2B), so Bralower et al. (2020) considered the observed 17 cm interval to be a minimum.

2. Methods

We scanned the cores at the XRF Core Scanning Lab at the IODP Gulf Coast Repository at Texas A&M University in College Station, TX. The archive halves of selected cores were scraped to ensure a fresh face of the core for scanning, and, in the case of the softer sediments of Site 95, to ensure a flat surface for the XRF core scanner (the split surface was generally smooth in the unlithified cores from Site 95 but decades in shrink wrap added a bit of texture in some places). Lithified sections from Sites 999 and 1001 were likewise scraped and leveled within the core liner to ensure a flat horizontal surface. Cores were then covered with 4 μm thick Ultralene film to prevent sediment from sticking to the scanner.

Cores were scanned on an Avaatech XRF Core Scanner at two excitation conditions focused on different element groups. The first scan was at 10kVp with no filter to analyze major and minor elements (Al, Si, K, Ca, Ti, Mn, Fe, Cr, P, S, and Mg) and the second was at 50kVp with a Cu filter to analyze heavier trace elements (Sr, Rb, Zr, and Ba). Scan resolution was set depending on relative distance above the K-Pg boundary, based on low resolution shipboard biostratigraphy. Core sections within Zone Pα or the lower part of Zone P1a (very roughly, within ~ 500 kyr after the boundary) were scanned at 1 or 2 cm steps, and sections below the boundary and >500 kyr after the boundary were scanned at 5 cm steps. Some steps were skipped or moved based on visual examination of the core before scanning (e.g., to avoid cracks or uneven surfaces). Laboratory standards were run at the beginning and end of each day to monitor instrumental performance.

Raw spectral data were processed into peak areas in the lab and exported as count data using the software program bAxil. Quality control of processed data was carried out using the following parameters: 1) throughput (samples with values <150,000 cps, which indicates a gap between the sensor and the core, were removed); 2) Argon peak (samples with positive Ar values, indicating that the sensor was measuring ambient air, were removed); and 3) standard deviation (samples with elemental peaks of Ba or Ti within 2 standard deviations of zero were removed).

To improve the age model for this study we analyzed planktic foraminifera from Site 95 at a resolution of up to 5 cm. Lightly lithified samples were gently broken into cm-sized pieces using a mortar and pestle. All samples were soaked in a solution of hydrogen peroxide and borax for at least 48 hours and then washed over a 45 μm sieve to ensure capture of typically very small early Paleocene taxa; the sieve was soaked in methylene blue dye between samples to mark contaminants. Finally, samples were dried overnight in an oven. Samples were examined for presence/absence of key marker species on a Zeiss Discovery.V8 light microscope. Species concepts follow those of Olsson et al., (1999); biozones are the Wade et al. (2011) update of the Paleocene biozonation scheme published by Berggren and Pearson (2005) and calibrated to the timescale of Gradstein et al. (2012).

3. Results

3.1 Biostratigraphy

Sediment at Site 95 is comprised of firm but unlithified calcareous ooze that yielded fairly well preserved material. We examined 25 samples from Cores 11 to 13 to identify and refine the boundaries between planktic foraminifer biozones. An obvious lithologic change occurs in Section 95-13R-3 at 24 cm (397.92 mbsf). Samples below this level are composed of mixed Cretaceous species remobilized by impact-induced seismic disturbance and tsunami, termed the K-Pg Boundary Cocktail (Bralower et al., 1998). From Sample 95-13R-2, 139 cm to Sample 95-13R-3, 24 cm (397.76 to 397.92 mbsf), the core is mottled and contains some signs of drilling disturbance (biscuiting, soft sediment deformation). Samples taken within what we interpret to be the biscuits, however, contain mostly Cretaceous species until 95-13R-3, 0-2 cm (397.70 mbsf), where the survivor species *Guembelitria cretacea* starts to become more common; this level is assigned to the base of Zone P0. The lowest occurrence of *P. eugubina,* which defines the base of Zone Pα, is found just above this level, in Sample 95-13R-2 130-132 cm (397.5 mbsf). The highest occurrence of *P. eugubina*, which marks the base of Zone P1a, occurs in sample 95-13R-1 130 cm (396.60 mbsf). Most of Zone P1a falls within a coring gap, but Zone Pα and the portion of Zone P1a preserved here contain abundant calcispheres, the resting cyst of calcareous dinoflagellates. Above the coring gap between Cores 95-12R and 13R, the bases of Zone P1b (lowest occurrence of *S. triloculinoides*) and Zone P1c (lowest occurrence of *Globanomalina compressa*) are both present. The base of Zone P2 (*P. uncinata*) is missing in another coring gap between Cores 11R and 12R, and the age model from the base of Zone P1c to the coring gap is based on extrapolating the sedimentation rate from Zone P1b; this method suggests that most of Zone P1c is present.

3.2 Ba/Ti

A key underlying assumption in the use of XRF scan data to reconstruct changes in biogenic Ba is that there is no change in the Ba/Ti value of terrigenous material delivered to the site. The extensive

volcanism documented in the Caribbean region throughout the early Cenozoic (Sigurdsson et al., 1997) could be a source of discrete or diffuse tephra deposition to the study sites which may vary through time and alter that ratio. Thus, we have plotted Ba from Site 999 and 1001 against Rb and Zr, which are enriched in volcanogenic minerals of the regional type of volcanism. Both Zr and Rb show weak positive correlation with Ba at Site 999 (Figure 3A-B) and a slightly less-weak positive correlation with Ba at Site 1001 (Figure 3C-D). This is to be expected, as any volcanic ash would have introduced more detrital Ba in the record. However, when we normalize Ba against Ti and compare this to Rb and Zr at both sites, the positive correlation goes away (Figure 3E-H). To demonstrate how overall changes in lithology affect Ba counts, we plotted Ba against Ca (any decrease in Ca in a pelagic setting above the lysocline is likely due to dilution by terrigenous material). At both sites, there is a weak negative correlation between Ca and Ba (Figure 3I-J). This is what we'd expect, as dilution of pelagic Ca by terrigenous material would introduce detrital Ba; this is why we normalize Ba to a terrigenous element like Ti. Overall, the relationship between Ca and Ba is not very strong, likely because overall terrigenous content in these pelagic clays is very low. We conclude that the Ba/Ti values at these sites do not reflect changes in terrigenous flux from either volcanism or other sources, and are thus primarily driven by changes in export productivity.

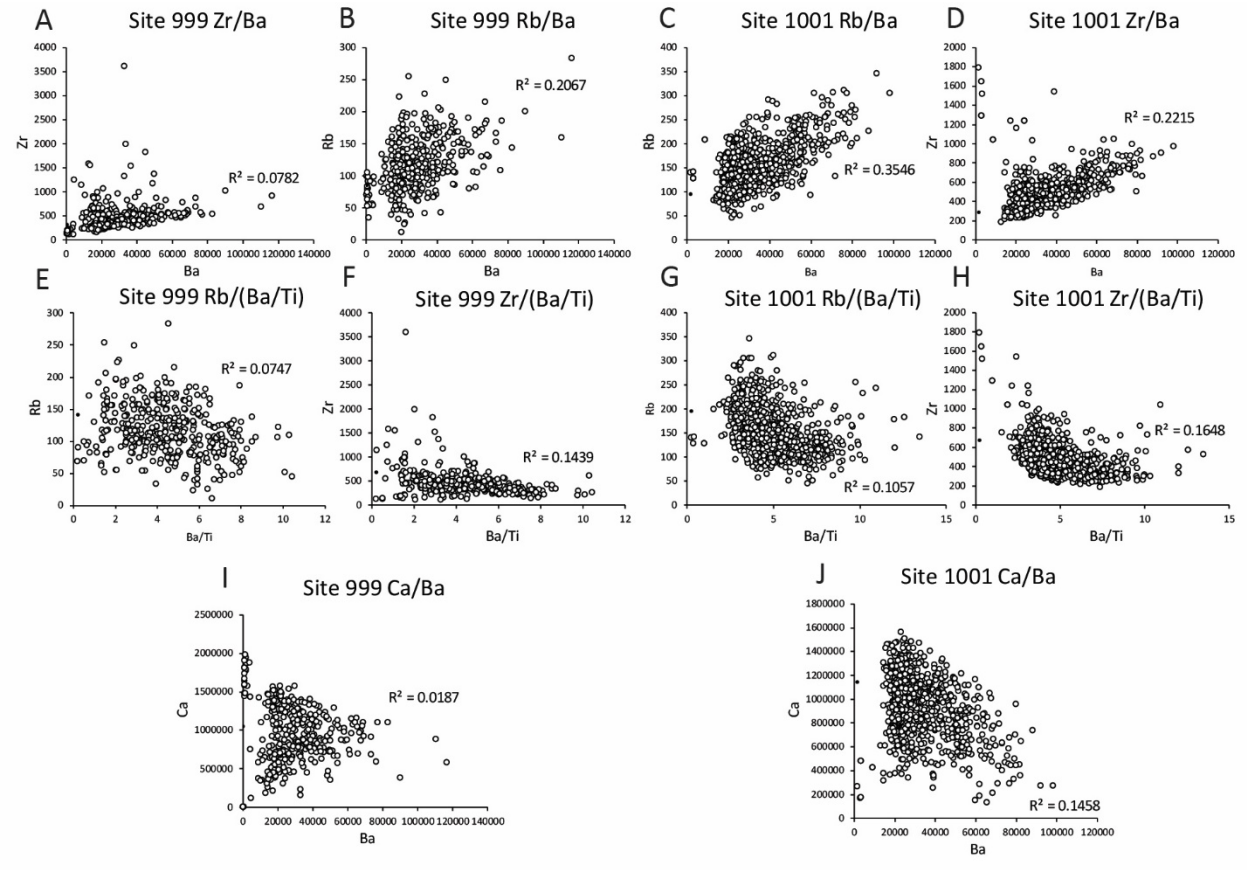

Figure 3. *Crossplots of Rb, Zr, and Ca with Ba and Ba/Ti from Sites 999 and 1001. R^2 values showing correlation (or lack thereof) for each parameter are included on the plots.*

3.2.1 Site M0077

Data from the Chicxulub Crater have been published (Lowery et al., 2018, 2021) but contain several interesting trends that should be summarized here. The highest Ba/Ti values in the study interval are found in the lowermost Paleocene, representing the first ~320 kyr after the impact (Figure 3A). At that point, there is a sharp drop in Ba/Ti values, followed by a steady decline from moderate values to a minimum about 1.2 myr after the K-Pg boundary, at which point values stabilize and remain low with some small-scale variability. Interestingly, this transition around 1.2 myr post-impact coincides with turnover in the calcareous nannoplankton ecosystem, as disaster taxa began to give way to acmes of new Paleocene taxa (Jones et al., 2019; Lowery et al., 2021).

3.2.2 Site 95

Ba/Ti values at Site 95 are also highest in the lowermost Paleocene, with a peak around the Pα/P1a zonal boundary and a sharp drop off ~340 kyr after the impact. A difference of 20 kyr between two sites whose age models are entirely based on biostratigraphy is basically within error and we feel comfortable assuming that this drop was contemporaneous with the one observed at Chicxulub Crater Site M0077. Approximately 300 kyr of the record in the middle of Zone P1a is erased by a coring gap, but above this level Ba/Ti values trend lower until about 1.1 myr after the K-Pg boundary. Values then remain low until about 1.6 myr post-impact and finally increase somewhat, varying through the rest of the record.

3.2.3 Site 1001

Site 1001 is the first of our sites in which there are data for the uppermost Cretaceous, and (above a gap where the boundary layer is mostly missing) Ba/Ti values increase in the Danian relative to the Maastrichtian. Although there is no obvious large peak like in the two Gulf of Mexico sites, there is an interval of overall higher values lasting to ~ 280 kyr after the impact. Above this level, values are much more variable than in the Gulf of Mexico but there is still a clear downward trend to a nadir around 1.4 myr after the K-Pg boundary, above which point values increase slightly and vary a little bit for the rest of the record.

3.2.4 Site 999

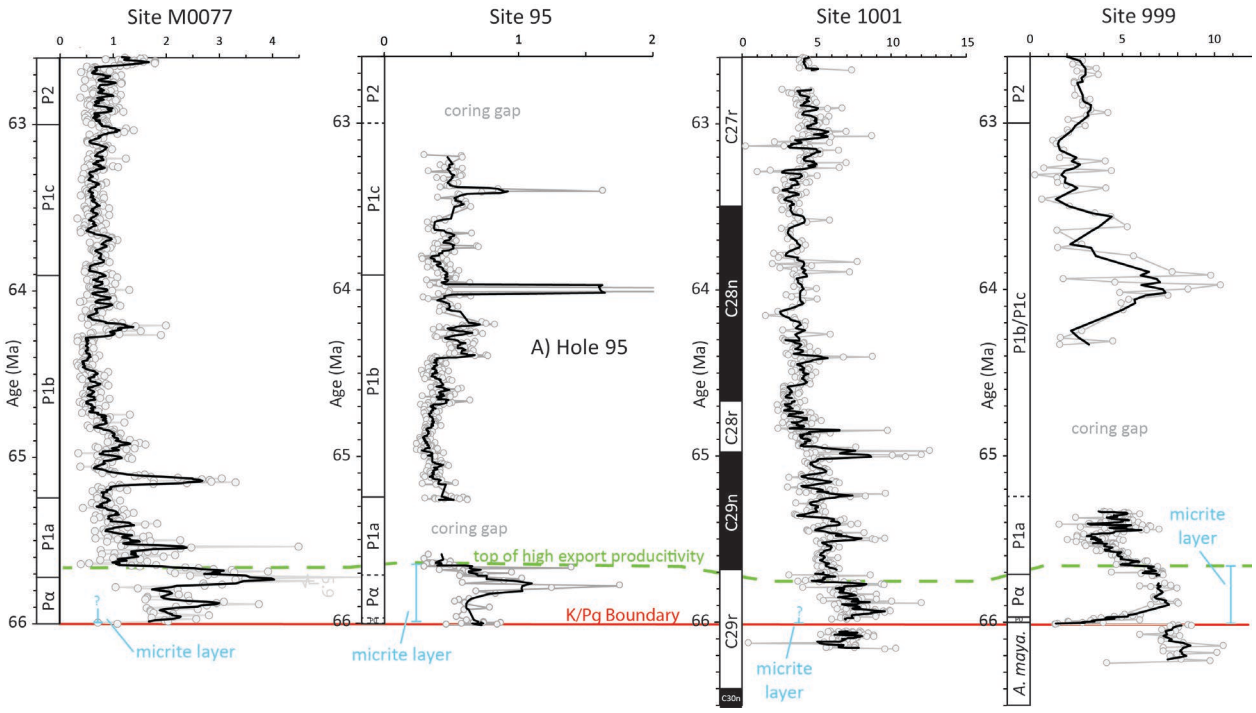

Figure 4. *Barium-Titanium export productivity proxy data for IODP Site M0077, DSDP Site 95, and ODP Sites 1001 and 999. Individual datapoints are grey circles, thick black lines is a 5-point moving average. Red line indicates the K-Pg boundary (or the top of the boundary interval in the case of Sites M0077 and 95), blue line indicates the thickness of the micrite layer identified at each site by Bralower et al. (2020), and the green dashed line indicates the top of the interval of highest export productivity at each site. PFZ: Planktic Foraminifer Zone (after Wade et al., 2011); A. maya.: Abathomphalus mayaroensis.*

Site 999 is the southernmost site, and the most distal from the Chicxulub impact crater. Ba/Ti values are very low directly above the boundary layer, quickly increasing through the lower part of Zone Pα. Higher values after this brief recovery interval do no exceed the Ba/Ti values observed in the uppermost Cretaceous, but they are much higher than subsequent Paleocene values (with the exception of a brief peak around 2 myr after the K-Pg boundary). Once again, values decreased sharply approximately 320 kyr post-impact followed by gradually declining values. The very poor quality of the biostratigraphy in this core (the Pα/P1a zonal boundary marker is the only reliable datum) makes it difficult to determine the timing of this decline and whether the increase observed below the coring gap occurred just 600 kyr after the boundary or much later. While we do not place much confidence in the ages above this level, we are confident in age control in the key interval above the boundary, specifically the highest occurrence of *P. eugubina* (Pα/P1a zonal boundary).

4. Discussion

4.1 Regional Homogeneity of Post K-Pg Export Production

The most striking feature of the four export productivity records presented here, and the key result of this investigation, is the consistent occurrence of relatively elevated Ba/Ti values in the earliest Paleocene. Interestingly, this is in line with trends from other sites in oligotrophic regions like the North Pacific Gyre. Three other open ocean sites have evidence of increased export productivity in the earliest Danian: the North Pacific Shatsky Rise and Hess Rise (Alegret and Thomas, 2005, 2009; Hull and Norris, 2011), and the mid-latitude South Pacific sections around Marlborough, South Island, New Zealand (Hollis et al., 1995, 2003). The high export productivity at Marlborough appears to be the result of increased upwelling along the continental margin (Hollis et al., 2003). Shatsky Rise and Hess Rise, though, are open ocean sites on roughly the same paleolatitude as our study area and were generally oligotrophic during this time interval (e.g., Deprez et al., 2017; Henehan et al., 2019). It is tempting to interpret the Ba/Ti data as elevated export production in the earliest Paleocene at all of these sites, in contrast with the overall global trend of reduced export production. But first we need to rule out other possible explanations.

As discussed above, there is no evidence that changes in terrigenous Ba/Ti values influence the record at our Caribbean sites, and could not explain how the same trend could be extended to the Gulf of Mexico and North Pacific sites. Likewise, we do not think transient (100-kyr-scale) changes in intermediate or deep water masses affecting barite dissolution rates make sense across such widely dispersed sites. The most likely explanations must be related to the oligotrophic gyres themselves, either oceanographic changes in the gyres or, more likely, ecological changes in the populations of phytoplankton and/or grazers in these gyres.

There are several possible mechanisms which could drive an increase in marine barite production while export production is kept steady. Different groups of plankton incorporate different amounts of Ba

423 into their biomass. For example, coccolithophores have less Ba in their cells than diatoms, which in turn
424 have less Ba in their cells than chrysophytes (gold algae), which have less Ba than chlorophytes (green
425 algae) (e.g., Paytan and Griffith, 2007). Calcareous nannoplankton suffered a severe extinction at the K-
426 Pg, and if they were briefly replaced in oligotrophic gyres by any of these other groups, the biogenic Ba
427 flux to the seafloor would increase even if export production held steady. Alternatively (or additionally),
428 an increase in temperature or a shift in bacterial ecology at mesopelagic depths could have increased
429 bacterial remineralization and thus barite production. A reduction in the abundance of grazers which
430 break apart sinking POM or an increase in ballasting or the formation of aggregates (which have the
431 effect of making POM sink more quickly) may have increased the amount of POM which sank below the
432 mesopelagic zone and to the seafloor. However, such a change wouldn't necessarily be expressed by
433 increased biogenic barium, since marine barite formation is a byproduct of the remineralization of organic
434 matter (Dehairs et al., 2008; Jacquet et al., 2011; Planchon et al., 2013) and quickly sinking POM has less
435 time to remineralize. On the other hand, a more robust grazer community at mesopelagic depths may have
436 broken apart more POM, slowed sinking and increased the time it was exposed to remineralization. Many
437 of these change (mesopelagic temperature increase, shifts in the grazer community or toward
438 phytoplankton with higher Ba abundance in their cells) are impossible to test with existing
439 paleoceanographic tools. What we can do, though, is look to other parts of the biological pump and see if
440 they indicate whether the observed increase in Ba/Ti was indeed related to export productivity.

441 Benthic foraminiferal accumulation rate and assemblages provide additional export productivity
442 information at these sites. Benthic foraminifera, which are responsive to the amount and quality of
443 organic matter that reaches the seafloor, record a different part of the biological pump than biogenic
444 barium, which is formed during the remineralization of organic matter at mesopelagic depths. Indeed,
445 these two proxies can sometimes show opposite trends (e.g., Griffith et al., 2021), which can help us
446 determine if our observations are the result of increased export production or some other process. At Site
447 M0077 in the Chicxulub Crater, elevated Ba/Ti values are associated with an interval of higher benthic

foraminiferal abundance, indicating increased export production was associated with increased food supply to the seafloor (Lowery et al., 2021). We don't have benthic foraminifera data from Site 95 because it is difficult to tell reworked benthics from *in situ* ones, and we don't have benthic foraminifera from Sites 999 and 1001 because of overall poor preservation of microfossils. On Shatsky Rise in the North Pacific gyre benthic foraminifera from Site 1210 (from Alegret and Thomas, 2009) and barium proxy data from the adjacent Site 577 (from Hull and Norris, 2011) are elevated for roughly the first 100 kyr after the extinction. On Hess Rise, also in the North Pacific gyre, no barium data exist but benthic foraminifera at Site 465 indicate a peak in post K-Pg burial flux within 100 kyr of the boundary (within planktic foraminifer Zone Pα) (Alegret and Thomas, 2005). At the three sites with both Ba and benthic foraminifer data, they both indicate increased transport of POM out of the euphotic zone and to the seafloor; we therefore interpret the Ba/Ti data at all our sites as primarily recording an increase in export productivity.

In the Gulf of Mexico and Caribbean, the interval of highest export production ends right around the Pα/P1a zonal boundary at each site, roughly 300 kyr after the K-Pg boundary, followed by a general decline over the next million years or so. The precise features vary from site to site; notably, the prominent early peak observed in the Gulf of Mexico (Sites M0077 and 95) is absent in the Caribbean cores (Sites 999 and 1001). Likewise, Site 999 records very low values immediately above the K-Pg boundary followed by a rapid recovery that is not evident at any of the other sites. Finally, the timing of the sharp decline of these high productivity intervals varies by a few tens of kyrs between sites. Because the age models are based on biostratigraphy *or* paleomagnetic reversals, with no higher resolution techniques like orbital chronology, it is impossible to say whether these differences are real or merely artifacts of the limits of the age models. These are superficial differences, though, and a clear overall trend exists that export productivity was elevated across Gulf of Mexico and Caribbean (a distance of ~1700 km) for ~300 kyr after the K-Pg mass extinction, and began to decline thereafter.

The observed homogeneity in regional export productivity in the earliest Paleocene provides important context for previous observations of global-scale heterogeneity determined with the Ba proxy. Previous work had shown major differences in the amount of organic matter remineralized in the mesopelagic zone between ocean basins, with an increase in export production in the middle of the North Pacific, a decline in the western North Atlantic, western South Atlantic, and Southern Ocean, and no change in the eastern South Atlantic (Hull and Norris, 2011). Those sites are widely separated and represent different oceanographic environments (oligotrophic gyres, western boundary currents, eastern boundary currents). With only one site in each region, it is hard to know whether these observations are indicative of regional trends or more limited, local change. With the discovery that open ocean sites within the Gulf of Mexico/Caribbean all exhibit the same trends (and, interestingly, the local change in benthic foraminiferal diversity in nearshore environments Gulf of Mexico is also lower than many other sites; Alegret et al., 2022), we can be more confident that previously observed regional differences are real, and therefore conclude that oligotrophic open ocean sites were prone to increased export production immediately after the K-Pg boundary, as suggested by Henehan et al. (2019). But what was the driver for this increased export production?

4.2 Drivers of Post-Extinction Export Productivity

In the modern ocean, oligotrophic gyres are typically dominated (in terms of biomass) by picophytoplankton (0.2-2.0 μm in size) like cyanobacteria and algae, but larger nano and micro phytoplankton (2-20 μm and >20 μm, respectively), though less numerous, account for the majority of productivity measured in incubation experiments (e.g., Marañón et al., 2003). Because picophytoplankton have no physical fossil record, we cannot say for sure whether this was the case at the end of the Cretaceous, but this seems like a safe assumption.

A switch from calcareous nannoplankton, the dominant phytoplankton of the Cretaceous (Bown, 2005) to smaller phytoplankton like cyanobacteria and chlorophyte algae would serve to reduce export flux globally and retain more nutrients in the euphotic zone, because smaller cell sizes sink more slowly

and are less likely to be consumed by zooplankton and packaged in fecal pellets, or bunch together in aggregates (Legrendre and Michaud, 1998; de la Rocha and Passow, 2007, although it should be noted that some modelling studies dispute the role of plankton size on export magnitude, e.g., Fakhraee et al., 2020). Henehan et al. (2019) pointed out that in oligotrophic regions, this post-extinction increase in nutrients could actually lead to an increase in primary and/or export productivity.

But how would NPP dominated by picophytoplankton lead to increased export production? After all, if export increased then there would be a mechanism to remove nutrients from the euphotic zone and NPP would necessarily decrease. Yet our work and that of others has found that high export production was maintained in typically oligotrophic regions for 100-300 kyr (Alegret and Thomas, 2005, 2009; Alegret et al., 2012, 2022; Hull and Norris, 2011). To explain this dichotomy, we suggest that POM exported from the euphotic zone became more refractory. The continuous remineralization of very small POM in the euphotic zone is termed the "microbial loop", and the only POM that manages to sink out of the euphotic zone is more refractory and difficult to metabolize (Legrendre and Michaud, 1998; de la Rocha and Passow, 2007). This refractory organic matter is less likely to be completely remineralized by grazers as it sinks through intermediate depths, which would result in less marine barite formation and lower Ba contents. However, if NPP increased after the K-Pg boundary at these sites as a result of the loss of larger phytoplankton, then the export of refractory POM may have increased, as would the amount of barite formation from that POM. Thus, even if only a small fraction of the refractory POM was remineralized, the overall increase in POM sinking below the euphotic zone would have elevated total remineralization and barite production. This also would explain why food supply increased to the seafloor, as evidenced by increases in benthic foraminifera.

An alternate explanation could be the occurrence of blooms of specific groups of phytoplankton with barium-rich cells or which favor barite formation. For example, in the modern ocean *Phaetocystis* is a common haptophyte which secretes extracellular polymers which form aggregates that speed sinking and enhance export production (e.g., Verity et al., 2007). These polymers may also play a key role in

marine barite formation as nucleation sites (Martinez-Ruiz et al., 2020). Acantharians have barium-rich skeletons and are known to form blooms in oligotrophic regions (e.g., Decelle et al., 2012) but, like the other groups, do not typically fossilize. Blooms of plankton like these may serve to increase export to the seafloor and also increase marine barite production without necessarily relying on a stronger microbial loop in the euphotic zone. While we currently lack direct evidence of blooms of non-fossilizing phytoplankton like these groups, more work is required to provide a clear answer to this question. But we can see some evidence for ecosystem changes associated with increased export productivity after the K-Pg.

4.3 Evidence of Ecosystem Changes

The second-most striking feature of our data is that at two of the sites studied (Sites 95 and 999) the interval of high export productivity ~300 kyr after the boundary coincides almost exactly with well-defined intervals of microcrystalline calcite ("micrite"). The widespread deposition of micrite in marine settings after the K-Pg boundary was documented by Bralower et al. (2020), and proposed to have been primarily formed by microbial blooms. The structure of individual micrite crystals is similar to that produced by various cyanobacteria (Bralower et al., 2020) and the micrite layer itself at several sites is associated with elevated biomarkers for photosynthetic bacteria and eukaryotic algae (Sepúlveda et al., 2009; Schaefer et al., 2020; Bralower et al., 2020). Some portion of the global micrite layer was also likely formed by the backreaction of CaO or CaOH vaporized by the Chicxulub impact, but this process would have been limited to the years after the impact as ejecta fell out of the atmosphere (Bralower et al., 2020) and wouldn't explain micrite deposition over ~300 kyr.

Extensive recrystallization of carbonate material at Site M0077 obscures the micrite record at that location. At Site M0077, abundant micrite is limited to a zone of good preservation which includes the "Transitional Unit" at the top of the K-Pg boundary layer (Morgan et al., 2017) and an overlying layer of green marlstone dated to the base of planktic foraminifer Zone Pα (Bralower et al., 2020). Above this, in the overlying white limestone layer, poor preservation prevents the consistent identification of micrite,

and so the top of the micrite layer is not identified. At Site 1001, coring gaps in the boundary interval in Hole 1001B limit the identification of the micrite layer to a minimum thickness (17 cm, Bralower et al., 2020). Thus, we have two sites showing a clear deposition of micrite ending at the same stratigraphic position (Sites 95 and 999), and two other sites with insufficient data to determine the relative timing (Sites M0077 and 1001).

None of the published Pacific sites which show an increase in post-K-Pg export production have both Ba/Ti data and micrite data (although we can compare nearby sites 1210 and 577 – see below). Micrite is enriched at Shatsky Rise Site 1209 over a 6 cm interval above the boundary, and at 1210 over a 7 cm interval above the boundary (Bralower et al., 2020), associated with the ~ 100 kyr peak in benthic foraminifer proxies for burial flux (Alegret and Thomas, 2009) and the ~ 100 kyr interval of elevated Ba/Ti at nearby Site 577 (Hull and Norris, 2011). At Hess Rise Site 465, micrite is enriched over a 24 cm interval above the boundary (Bralower et al., 2020), and benthic foraminifera likewise show a peak in burial flux in this interval (Alegret and Thomas, 2005). It is important to point out that foraminifer samples at both Sites 465 and 1210 were taken at a 10 cm resolution (Alegret and Thomas, 2005, 2009) so a precise tie between the decline in export productivity and the end of micrite deposition is impossible to make.

Although various types of "ballast," including calcite plankton shells, have been thought to influence export production in the modern ocean (Armstrong et al., 2001; Francois et al., 2002), it does not seem likely that micrite itself, or more specifically the cyanobacteria that produced it, is the cause of increased export production in the earliest Paleocene. Micrite is abundant at many sites which did not experience elevated export production after the K-Pg. For example, Blake Nose Site 1049, which experienced either a decline or no change in export production after the boundary (Alegret and Thomas, 2004), has a 30 cm thick micrite layer. Walvis Ridge Site 1262, which similarly experienced no change in post-extinction export production based on benthic foraminifera (Alegret and Thomas, 2007), has a 1.82 m thick micrite layer. All told, Bralower et al. (2020) identified micrite layers at 31 sites globally; of

these, only 5 record elevated export production in the early Danian based on available proxies. All of these sites are in open ocean settings which are predisposed to oligotrophy.

The general association of the micrite layer (indicating dominance of microbial primary producers) with the elevated post-impact export production across Pacific and Caribbean/Gulf of Mexico sites suggests that a post-extinction dominance of picophytoplankton is the primary mechanism driving elevated export productivity at previously oligotrophic parts of the open ocean in the earliest Paleocene.

The dominance of picophytoplankton may have been the proximal cause of elevated post K-Pg export production in tropical open ocean waters, but it is important to note that the timing was different between the Caribbean and the central Pacific. The period of highest export production dropped off ~ 300 kyr after the K-Pg in the Gulf of Mexico and Caribbean but much earlier at Shatsky and Hess Rises, i.e., after ~ 100 kyr (Alegret and Thomas, 2005, 2009; Hull and Norris, 2011). This is in line with previous results which indicate a global diachroneity in the turnover of calcareous nannoplankton assemblages in the earliest Paleocene (Jones et al., 2019), driven by transition from surface waters characterized by efficient recycling of nutrients due to the prevalence of picophytoplankton feeding the microbial loop, to surface waters characterized by less efficient recycling of nutrients caused by greater export of larger plankton out of the euphotic zone (Jones et al., 2019; Lowery et al., 2021). At Shatsky Rise, disaster assemblages of calcareous nannoplankton gave way to acmes of Paleocene taxa soon after the K-Pg (Alvarez et al., 2019; Jones et al., 2019). On the other hand, disaster taxa in the Chicxulub Crater continued until the final decline in export productivity about a million years after the K-Pg (Jones et al., 2019), and at Site 999, disaster taxa continued at least into Zone P1a >300 kyr after the K-Pg (Sigurdsson et al., 1997). Whether the recovery in calcareous nannoplankton caused the observed change in export production or if a reduction in export production spurred the local diversification of calcareous nannoplankton remains an open question.

Conclusions

Our XRF-derived Ba/Ti export productivity proxy data from the Gulf of Mexico and Caribbean show a post K-Pg peak in export productivity across the region, with an interval of high values lasting for ~ 300 kyr after the boundary, then declining values for another ~ 700 kyr. This is a major improvement on previous compilations of earliest Paleocene export productivity, which showed that post-extinction changes in export production were globally heterogeneous on an ocean basin scale. Our results show that broad regions followed similar trends. In particular, we find that most elevated export production in the earliest Danian occurred tropical open ocean sites (Shatsky Rise, Hess Rise, and our Caribbean/Gulf of Mexico sites) which were oligotrophic at the end of the Cretaceous (Henehan et al., 2019).

At sites with elevated export production and at which preservation makes such observations possible, the post K-Pg global micrite layer corresponds to the interval of elevated export production. We interpret this as evidence that the dominance of picophytoplankton like cyanobacteria and chlorophyte algae, which appear to have been responsible for the micrite deposition (Bralower et al., 2020), altered the dynamics of the biological pump to increase recycling of organic matter in the euphotic zone. Enhanced recycling of organic matter left only refractory material, which is more difficult to recycle, to be exported from the euphotic zone. Because it is refractory, this organic matter would have been more likely to sink through the water column than more labile material exported under normal conditions. In typically oligotrophic environments, this slight increase in efficiency of the biologic pump could have resulted in overall higher export production; as larger phytoplankton recovered and more labile organic matter was exported and grazed, enhanced export production would have subsided.

More datasets from a wider range of latitudes and ocean basins are needed to build a more complete picture of post K-Pg export production to more fully understand how the marine biosphere recovered from the most recent major mass extinction.

Open Research

XRF core scan data and age models are archived at the NCEI Paleoclimate Database (Lowery, 2021).

Acknowledgements

We are grateful for insightful reviews by Ellen Thomas and an anonymous reviewer, both of which substantially improved this manuscript. We are also grateful to Brian LeVay and Mackenzie Schoemann of the IODP Gulf Coast Repository (GCR) at Texas A&M University for their assistance with XRF core scanning, the staff of the GCR for sending samples from Sites 95 and 536 for biostratigraphic analysis, and Vinny Percuoco at the GCR for providing high resolution photograph for the K-Pg boundary in Hole 1001B. We are also grateful to Ryan Weber and Calvin Gordon of PaleoData, Inc., for their assistance preparing samples from Site 999 and 1001 for biostratigraphic analysis.

Figure 1. A) Global plate tectonic reconstruction from 66 Ma showing location of our study area (in red) and other notable sites discussed in this paper (in orange). Grey areas are continental blocks, terranes, and plateaus; map from ODSN generated at https://www.odsn.de/odsn/services/paleomap/paleomap.html. B) Regional map showing position of our study sites around the time of the K-Pg Boundary. Map modified after Pindell and Barrett (1990) and Snedden et al. (2021). Black indicates land and grey indicates shelves.

Figure 2. Stratigraphic sections showing lithostratigraphy, core scan photographs, and images of the K-Pg boundary of the studied intervals from DSDP Hole 95, ODP Hole 1001A, and ODP Hole 999B. Lithostratigraphy follows shipboard descriptions Worzel, Bryant et al. (1973) for Site 95 and Sigurdsson et al., 1997 for Sites 999 and 1001). Core scan photographs were collected at the GCR at the same time XRF data were collected (except for the photograph of the K-Pg boundary in Hole 1001B, which is from the ODP photo archives). Mbsf = meters below sea floor, PFZ = Planktic Foraminifer Zone, Lith. = lithology, PMag = Paleomagnetic polarity, E. Campanian = Early Campanian, Maas. = Maastrichtian, *G. elevata* = *Globotruncanita elevata, A.m.* and *A. mayaroensis* = *Abathomphalus mayaroensis*.

643 **Figure 3.** Crossplots of Rb, Zr, and Ca with Ba and Ba/Ti ratios from Sites 999 and 1001. R^2 values
644 showing correlation (or lack thereof) for each parameter are included on the plots.

645

646 **Figure 4.** Barium/Titanium export productivity proxy data for IODP Site M0077, DSDP Site 95, and
647 ODP Sites 1001 and 999. Individual datapoints are grey circles, thick black lines are a 5-point moving
648 average. Red line indicates the K-Pg boundary (or the top of the boundary interval in the case of Sites
649 M0077 and 95), blue line indicates the thickness of the micrite layer identified at each site by Bralower et
650 al. (2020), and the green dashed line indicates the top of the interval of highest export productivity at each
651 site. PFZ = Planktic Foraminifer Zone, *A. maya. = Abathomphalus mayaroensis*.

652 **References**

653 Alegret, L. & Thomas, E. (2004). Benthic foraminifera and environmental turnover across the
654 Cretaceous/Paleogene boundary at Blake Nose (ODP Hole 1049C, Northwestern Atlantic).
655 Palaeogeography, Palaeoclimatology, Palaeoecology, 208: 59-83; doi:
656 10.1016/j.palaeo.2004.02.028

657 Alegret, L., & Thomas, E. (2005). Cretaceous/Paleogene boundary bathyal paleo-environments in the
658 central North Pacific (DSDP Site 465), the Northwestern Atlantic (ODP Site 1049), the Gulf of
659 Mexico and the Tethys: The benthic foraminiferal record. Palaeogeography, Palaeoclimatology,
660 Palaeoecology, 224(1-3), 53-82.

661 Alegret, L., & Thomas, E. (2007). Deep-sea environments across the Cretaceous/Paleogene boundary in
662 the eastern South Atlantic Ocean (ODP leg 208, Walvis Ridge). Marine Micropaleontology, 64(1-
663 2), 1-17.

664 Alegret, L., & Thomas, E. (2009). Food supply to the seafloor in the Pacific Ocean after the
665 Cretaceous/Paleogene boundary event. Marine Micropaleontology, 73(1-2), 105-116.

Alegret, L., Thomas, E., & Lohmann, K. C. (2012). End-Cretaceous marine mass extinction not caused by productivity collapse. Proceedings of the National Academy of Sciences, 109(3), 728-732.

Alegret, L., Arreguín-Rodríguez, G. J., Trasviña-Moreno, C. A., & Thomas, E. (2021). Turnover and stability in the deep sea: Benthic foraminifera as tracers of Paleogene global change. *Global and Planetary Change*, *196*, 103372.

Alegret, L., Arreguin-Rodriguez, G., and Thomas, E., 2022. Oceanic productivity after the Cretaceous/Paleogene impact: where do we stand? The view from the deep. in Koeberl, C., Claeys, P., and Montanari, A., eds., From the Guajira Desert to the Apennines, and from Mediterranean Microplates to the Mexican Killer Asteroid: Honoring the Career of Walter Alvarez: *Geological Society of America Special Paper* 557, https://doi.org/10.1130/2022.2557(21)

Alvarez, L. W., Alvarez, W., Asaro, F., & Michel, H. V. (1980). Extraterrestrial cause for the Cretaceous-Tertiary extinction. *Science*, *208*(4448), 1095-1108.

Alvarez, S. A., Gibbs, S. J., Bown, P. R., Kim, H., Sheward, R. M., & Ridgwell, A. (2019). Diversity decoupled from ecosystem function and resilience during mass extinction recovery. *Nature*, *574*(7777), 242-245.

Armstrong, R. A., Lee, C., Hedges, J. I., Honjo, S., & Wakeham, S. G. (2001). A new, mechanistic model for organic carbon fluxes in the ocean based on the quantitative association of POC with ballast minerals. Deep Sea Research Part II: Topical Studies in Oceanography, 49(1-3), 219-236.

Artemieva, N., Morgan, J., & Expedition 364 Science Party. (2017). Quantifying the release of climate-active gases by large meteorite impacts with a case study of Chicxulub. Geophysical Research Letters, 44(20), 10-180.

688 Artemieva, N., & Morgan, J. (2020). Global K-Pg layer deposited from a dust cloud. Geophysical
689 Research Letters, 47(6), e2019GL086562.

690 Bains, S., Norris, R. D., Corfield, R. M., & Faul, K. L. (2000). Termination of global warmth at the
691 Palaeocene/Eocene boundary through productivity feedback. Nature, 407(6801), 171-174.

692 Bardeen, C. G., Garcia, R. R., Toon, O. B., & Conley, A. J. (2017). On transient climate change at the
693 Cretaceous− Paleogene boundary due to atmospheric soot injections. Proceedings of the National
694 Academy of Sciences, 114(36), E7415-E7424.

695 Barton, A. D., Irwin, A. J., Finkel, Z. V., & Stock, C. A. (2016). Anthropogenic climate change drives
696 shift and shuffle in North Atlantic phytoplankton communities. Proceedings of the National
697 Academy of Sciences, 113(11), 2964-2969.

698 Berggren, W. A., & Pearson, P. N. (2005). A revised tropical to subtropical Paleogene planktonic
699 foraminiferal zonation. The Journal of Foraminiferal Research, 35(4), 279-298.

700 Birch, H. S., Coxall, H. K., Pearson, P. N., Kroon, D., & Schmidt, D. N. (2016). Partial collapse of the
701 marine carbon pump after the Cretaceous-Paleogene boundary. Geology, 44(4), 287-290.

702 Birch, H., Schmidt, D. N., Coxall, H. K., Kroon, D., & Ridgwell, A. (2021). Ecosystem function after the
703 K/Pg extinction: decoupling of marine carbon pump and diversity. Proceedings of the Royal
704 Society B, 288(1953), 20210863.

705 Bown, P. (2005). Selective calcareous nannoplankton survivorship at the Cretaceous-Tertiary boundary.
706 Geology, 33(8), 653-656.

707 Boyd, P. W., & Trull, T. W. (2007). Understanding the export of biogenic particles in oceanic waters: Is
708 there consensus?. Progress in Oceanography, 72(4), 276-312.

709 Bralower, T. J., Paull, C. K., & Mark Leckie, R. (1998). The Cretaceous-Tertiary boundary cocktail:
710 Chicxulub impact triggers margin collapse and extensive sediment gravity flows. Geology, 26(4),
711 331-334.

712 Bralower, T. J., Cosmidis, J., Heaney, P. J., Kump, L. R., Morgan, J. V., Harper, D. T., ... & Vajda, V.
713 (2020). Origin of a global carbonate layer deposited in the aftermath of the Cretaceous-Paleogene
714 boundary impact. Earth and Planetary Science Letters, 548, 116476.

715 Brugger, J., Feulner, G., & Petri, S. (2017). Baby, it's cold outside: Climate model simulations of the
716 effects of the asteroid impact at the end of the Cretaceous. *Geophysical Research Letters*, *44*(1),
717 419-427.

718 Buesseler, K. O., & Boyd, P. W. (2009). Shedding light on processes that control particle export and flux
719 attenuation in the twilight zone of the open ocean. Limnology and Oceanography, 54(4), 1210-
720 1232.

721 Buffler, R.T., Schlager, W., et al. (1984). Initial Reports of the Deep Sea Drilling Project 77,
722 doi:10.2973/dsdp.proc.77.1984

723 Coxall, H. K., D'Hondt, S., & Zachos, J. C. (2006). Pelagic evolution and environmental recovery after
724 the Cretaceous-Paleogene mass extinction. Geology, 34(4), 297-300.

725 Culver, S. J. (2003). Benthic foraminifera across the Cretaceous–Tertiary (K–T) boundary: a review.
726 Marine Micropaleontology, 47(3-4), 177-226.

727 D'Hondt, S., Donaghay, P., Zachos, J. C., Luttenberg, D., & Lindinger, M. (1998). Organic carbon fluxes
728 and ecological recovery from the Cretaceous-Tertiary mass extinction. Science, 282(5387), 276-
729 279.

730 De La Rocha, C. L., & Passow, U. (2007). Factors influencing the sinking of POC and the efficiency of
731 the biological carbon pump. Deep Res II 54: 639–658.

Decelle, J., Probert, I., Bittner, L., Desdevises, Y., Colin, S., de Vargas, C., Galí, M., Simó, R. and Not, F., 2012. An original mode of symbiosis in open ocean plankton. *Proceedings of the National Academy of Sciences*, *109*(44), pp.18000-18005.

Dehairs, F., Jacquet, S., Savoye, N., Van Mooy, B. A., Buesseler, K. O., Bishop, J. K. B., Lamborg, C. H., Elskens, M., Baeyens, W., Bowd, P. W., Cascotti, K.L., & Monnin, C. (2008). Barium in twilight zone suspended matter as a potential proxy for particulate organic carbon remineralization: Results for the North Pacific. *Deep Sea Research Part II: Topical Studies in Oceanography*, *55*(14-15), 1673-1683.

Deprez, A., Jehle, S., Bornemann, A., & Speijer, R. P. (2017). Pronounced biotic and environmental change across the latest Danian warming event (LDE) at Shatsky Rise, Pacific Ocean (ODP Site 1210). *Marine Micropaleontology*, *137*, 31-45.

Denne, R. A., Scott, E. D., Eickhoff, D. P., Kaiser, J. S., Hill, R. J., & Spaw, J. M. (2013). Massive Cretaceous-Paleogene boundary deposit, deep-water Gulf of Mexico: New evidence for widespread Chicxulub-induced slope failure. Geology, 41(9), 983-986.

Doyle, P. S., & Riedel, W. R. (1979). Ichthyoliths: present status of taxonomy and stratigraphy of microscopic fish skeletal debris. Scripps Institution of Oceanography, University of California at San Diego.

Dymond, J., Suess, E., & Lyle, M. (1992). Barium in deep-sea sediment: A geochemical proxy for paleoproductivity. Paleoceanography, 7(2), 163-181.

Eagle, M., Paytan, A., Arrigo, K. R., van Dijken, G., & Murray, R. W. (2003). A comparison between excess barium and barite as indicators of carbon export. Paleoceanography, 18(1).

753 Esmeray-Senlet, S., Wright, J. D., Olsson, R. K., Miller, K. G., Browning, J. V., & Quan, T. M. (2015).
754 Evidence for reduced export productivity following the Cretaceous/Paleogene mass extinction.
755 Paleoceanography, 30(6), 718-738.

756 Fakhraee, M., Planavsky, N. J., & Reinhard, C. T. (2020). The role of environmental factors in the long-
757 term evolution of the marine biological pump. *Nature Geoscience*, *13*(12), 812-816.

758 Fraass, A. J., Kelly, D. C., & Peters, S. E. (2015). Macroevolutionary history of the planktic foraminifera.
759 Annual Review of Earth and Planetary Sciences, 43, 139-166.

760 Francois, R., Honjo, S., Manganini, S. J., & Ravizza, G. E. (1995). Biogenic barium fluxes to the deep
761 sea: Implications for paleoproductivity reconstruction. Global Biogeochemical Cycles, 9(2), 289-
762 303.

763 Francois, R., Honjo, S., Krishfield, R., & Manganini, S. (2002). Factors controlling the flux of organic
764 carbon to the bathypelagic zone of the ocean. Global Biogeochemical Cycles, 16(4), 34-1.

765 Gibbs, S. J., Bown, P. R., Ward, B. A., Alvarez, S. A., Kim, H., Archontikis, O. A., Sauterey, B. Poulton, A.
766 J., Wilson, J., & Ridgwell, A. (2020). Algal plankton turn to hunting to survive and recover from
767 end-Cretaceous impact darkness. *Science advances*, *6*(44), eabc9123.

768 Gradstein, F. M., Ogg, J. G., Schmitz, M. D., & Ogg, G. M. (Eds.). (2012). The geologic time scale 2012.
769 elsevier.

770 Griffith, E. M., & Paytan, A. (2012). Barite in the ocean–occurrence, geochemistry and
771 palaeoceanographic applications. Sedimentology, 59(6), 1817-1835.

772 Griffith, E. M., Thomas, E., Lewis, A. R., Penman, D. E., Westerhold, T., & Winguth, A. M. (2021).
773 Bentho-Pelagic Decoupling: The Marine Biological Carbon Pump During Eocene
774 Hyperthermals. *Paleoceanography and Paleoclimatology*, *36*(3), e2020PA004053.

775 Hallock, P. (1987). Fluctuations in the trophic resource continuum: a factor in global diversity cycles?.
776 Paleoceanography, 2(5), 457-471.

777 Henehan, M. J., Ridgwell, A., Thomas, E., Zhang, S., Alegret, L., Schmidt, D. N., Rae, J. W. B., Witts, J.
778 D., Landman, N. H., Greene, S. E., & Hull, P. M. (2019). Rapid ocean acidification and
779 protracted Earth system recovery followed the end-Cretaceous Chicxulub impact. Proceedings of
780 the National Academy of Sciences, 116(45), 22500-22504.

781 Henson, S. A., Sanders, R., & Madsen, E. (2012). Global patterns in efficiency of particulate organic
782 carbon export and transfer to the deep ocean. Global Biogeochemical Cycles, 26(1).

783 Hollis, C. J., Rodgers, K. A., & Parker, R. J. (1995). Siliceous plankton bloom in the earliest Tertiary of
784 Marlborough, New Zealand. Geology, 23(9), 835-838.

785 Hollis, C. J., Strong, C. P., Rodgers, K. A., & Rogers, K. M. (2003). Paleoenvironmental changes across
786 the Cretaceous/Tertiary boundary at Flaxbourne River and Woodside Creek, eastern
787 Marlborough, New Zealand. New Zealand Journal of Geology and Geophysics, 46(2), 177-197.

788 Hsü, K. J., He, Q., McKenzie, J. A., Weissert, H., Perch-Nielsen, K., Oberhänsli, H., Kelts, K.,
789 LaBrecque, J., Tauxe, L., Krähenbühl, R., Percival, Jr., S. F., Wright, R., Karpoff, A. M.,
790 Petersen, S. F., Tucker, P., Poor, R. Z., Gombos, A. M., Posciotto, K., Carman, Jr., M. F., &
791 Schreiber, E. (1982). Mass mortality and its environmental and evolutionary
792 consequences. *Science*, *216*(4543), 249-256.

793 Hsü, K. J., & Mckenzie, J. A. (1985). A “Strangelove” ocean in the earliest Tertiary. The Carbon Cycle
794 and Atmospheric CO2: Natural Variations Archean to Present, 32, 487-492.

795 Hull, P. M., & Norris, R. D. (2011). Diverse patterns of ocean export productivity change across the
796 Cretaceous-Paleogene boundary: New insights from biogenic barium. Paleoceanography, 26(3).

797 Jacquet, S. H., Dehairs, F., Dumont, I., Becquevort, S., Cavagna, A. J., & Cardinal, D. (2011). Twilight
798 zone organic carbon remineralization in the Polar Front Zone and Subantarctic Zone south of
799 Tasmania. *Deep Sea Research Part II: Topical Studies in Oceanography*, *58*(21-22), 2222-2234.

800 Jiang, S., Bralower, T. J., Patzkowsky, M. E., Kump, L. R., & Schueth, J. D. (2010). Geographic controls
801 on nannoplankton extinction across the Cretaceous/Palaeogene boundary. Nature Geoscience,
802 3(4), 280-285.

803 Jones, H. L., Lowery, C. M., & Bralower, T. J. (2019). Delayed calcareous nannoplankton boom-bust
804 successions in the earliest Paleocene Chicxulub (Mexico) impact crater. Geology, 47(8), 753-756.

805 Jonkers, L., Hillebrand, H., & Kucera, M. (2019). Global change drives modern plankton communities
806 away from the pre-industrial state. *Nature*, *570*(7761), 372-375.

807 Kump, L. R. (1991). Interpreting carbon-isotope excursions: Strangelove oceans. *Geology*, *19*(4), 299-
808 302.

809 Legendre, L., & Michaud, J. (1998). Flux of biogenic carbon in oceans: size-dependent regulation by
810 pelagic food webs. *Marine Ecology Progress Series*, *164*, 1-11.

811 Louvel, V., & Galbrun, B. (2000). Magnetic polarity sequences from downhole measurements in ODP
812 holes 998B and 1001A, leg 165, Caribbean Sea. Marine Geophysical Researches, 21(6), 561-577.

813 Lowery, C. M., Bralower, T. J., Owens, J. D., Rodríguez-Tovar, F. J., Jones, H., Smit, J., Whalen, M. T.,
814 Claeys, P., Farley, K., Gulick, S. P. S., Morgan, J. V., Green, S., Chenot, E., Christeson, G. L.,
815 Cockell, C. S. Coolen, M. J. L., Ferrière, L., Gebhardt, C., Goto, K., Kring, D. A., Lofi, J.,
816 Ocampo-Torres, R., Perez-Cruz, L., Pickersgill, A. E., Poelchau, M. H., Rae, A. S. P., Rasmussen
817 C., Rebolledo-Vieyra, M., Riller, U., Sato, H., Tikoo, S. M., Tomioka, N., Urrutia-Fucugauchi, J.,
818 Vellekoop, J., Wittmann, A., Xiao, L., Yamaguchi, K. E., & Zylberman, W. (2018). Rapid
819 recovery of life at ground zero of the end-Cretaceous mass extinction. Nature, 558(7709), 288-
820 291.

Lowery, C. M., Bown, P. R., Fraass, A. J., & Hull, P. M. (2020). Ecological response of plankton to environmental change: thresholds for extinction. Annual Review of Earth and Planetary Sciences, 48, 403-429.

Lowery, C.M. (2021): NOAA/WDS Paleoclimatology - Gulf of Mexico and Caribbean XRF Core Scan Data from the Early Paleocene. [Dataset]. NOAA National Centers for Environmental Information. https://doi.org/10.25921/g1wy-1d88.

Lowery, C. M., Jones, H., Bralower, T. J., Perez Cruz, L., Gebhardt, C., Whalen, M. T., Chenot, E., Smit, J., Purkey Phillips, M., Choumiline, K., Arenillas, I., Arz, J. A., Garcia, F., Ferrand, M., Gulick, S. P. S., and IODP Expedition 364 Scientists. (2021) Early Paleocene paleoceanography and export productivity in the Chicxulub crater. Paleoceanography & Paleoclimatology.

Marañón, E., Behrenfeld, M. J., González, N., Mouriño, B., & Zubkov, M. V. (2003). High variability of primary production in oligotrophic waters of the Atlantic Ocean: uncoupling from phytoplankton biomass and size structure. *Marine Ecology Progress Series*, *257*, 1-11.

Martinez-Ruiz, F., Paytan, A., Gonzalez-Muñoz, M. T., Jroundi, F., Abad, M. D. M., Lam, P. J., Horner, T. J., & Kastner, M. (2020). Barite precipitation on suspended organic matter in the mesopelagic zone. *Frontiers in Earth Science*, *8*, 567714.

Molina, E., Alegret, L., Arenillas, I., Arz, J. A., Gallala, N., Hardenbol, J., von Salis, K., Steurbaut, E., Vandenberghe, N., & Zaghbib-Turki, D. (2006). The global boundary stratotype section and point for the base of the Danian stage (Paleocene, Paleogene," Tertiary", Cenozoic) at El Kef, Tunisia-original definition and revision. Episodes, 29(4), 263.

Moore, J.K., Fu, W., Primeau, F., Britten, G.L., Lindsay, K., Long, M., Doney, S.C., Mahowald, N., Hoffman, F. and Randerson, J.T., 2018. Sustained climate warming drives declining marine biological productivity. *Science*, *359*(6380), pp.1139-1143.

844 Morgan, J., Gulick, S., Mellett, C. L., & Green, S. L. (2017). Chicxulub: drilling the K-Pg impact crater.
845 Proceedings of the International Ocean Discovery Program, 364.
846 https://doi.org/10.14379/iodp.proc.364.2017

847 Müller, P. J. and Suess, E., 1979. Productivity, sedimentation rate, and sedimentary organic matter in the
848 oceans—I. Organic carbon preservation. Deep Sea Research Part A. Oceanographic Research
849 Papers, 26(12), pp.1347-1362.

850 Olsson, R. K., Berggren, W. A., Hemleben, C., & Huber, B. T. (1999). Atlas of Paleocene planktonic
851 foraminifera. Smithsonian Contributions to Paleobiology 85, 1-106

852 Passow, U., & Carlson, C. A. (2012). The biological pump in a high CO_2 world. *Marine Ecology*
853 *Progress Series*, *470*, 249–272. http://www.jstor.org/stable/24876215

854 Paytan, A., Kastner, M., & Chavez, F. P. (1996). Glacial to interglacial fluctuations in productivity in the
855 equatorial Pacific as indicated by marine barite. Science, 274(5291), 1355-1357.

856 Paytan, A., & Griffith, E. M. (2007). Marine barite: Recorder of variations in ocean export productivity.
857 Deep Sea Research Part II: Topical Studies in Oceanography, 54(5-7), 687-705.

858 Paytan, A., Averyt, K., Faul, K., Gray, E., & Thomas, E. (2007). Barite accumulation, ocean productivity,
859 and Sr/Ba in barite across the Paleocene-Eocene Thermal Maximum. Geology, 35: 1139-1142

860 Pindell, J. L., & Barrett, S. F. (1990). Caribbean plate tectonic history. *The Caribbean Region, volume H*
861 *of The Geology of North America*, 405-432.

862 Planchon, F., Cavagna, A. J., Cardinal, D., André, L., & Dehairs, F. (2013). Late summer particulate
863 organic carbon export and twilight zone remineralisation in the Atlantic sector of the Southern
864 Ocean. *Biogeosciences*, *10*(2), 803-820.

865 Sanford, J. C., Snedden, J. W., & Gulick, S. P. (2016). The Cretaceous-Paleogene boundary deposit in the
866 Gulf of Mexico: Large-scale oceanic basin response to the Chicxulub impact. Journal of
867 Geophysical Research: Solid Earth, 121(3), 1240-1261.

868 Schaefer, B., Grice, K., Coolen, M. J., Summons, R. E., Cui, X., Bauersachs, T., Böttcher, M.E.,
869 Bralower, T.J., Lyons, S.L. and Freeman, K.H, Cockell, C. S., Gulick, S. P. S., Morgan, J. V.,
870 Whalen, M. T., Lowery, C. M., & Vajda, V. (2020). Microbial life in the nascent Chicxulub
871 crater. Geology, 48(4), 328-332.

872 Schueth, J. D., Bralower, T. J., Jiang, S., & Patzkowsky, M. E. (2015). The role of regional survivor
873 incumbency in the evolutionary recovery of calcareous nannoplankton from the
874 Cretaceous/Paleogene (K/Pg) mass extinction. Paleobiology, 41(4), 661-679.

875 Sepúlveda, J., Wendler, J. E., Summons, R. E., & Hinrichs, K. U. (2009). Rapid resurgence of marine
876 productivity after the Cretaceous-Paleogene mass extinction. Science, 326(5949), 129-132.

877 Sepúlveda, J., Alegret, L., Thomas, E., Haddad, E., Cao, C., & Summons, R. E. (2019). Stable isotope
878 constraints on marine productivity across the Cretaceous-Paleogene mass extinction.
879 Paleoceanography and Paleoclimatology, 34(7), 1195-1217.

880 Sibert, E. C., & Norris, R. D. (2015). New Age of Fishes initiated by the Cretaceous− Paleogene mass
881 extinction. Proceedings of the National Academy of Sciences, 112(28), 8537-8542.

882 Sigurdsson, H., Leckie, R.M., Acton, G.D., et al., 1997. Proceedings of the Ocean Drilling Program,
883 Initial Reports., 165: College Station, TX (Ocean Drilling Program).
884 doi:10.2973/odp.proc.ir.165.1997

885 Snedden, J., Leshyk, V. O., and Kring, D. (2021). Paleogeographic Evolution of the Chicxulub Region.
886 Lunar and Planetary Institute illustration,
887 https://www.lpi.usra.edu/exploration/training/illustrations/chicxulub-effects/, accessed 9/27/21.

888 Thierstein, H. R. (1982). Terminal Cretaceous plankton extinctions: A critical assessment. Geological
889 implications of impacts of large asteroids and comets on the earth, 190, 385-399.

890 Thomas, E., 1990. Late Cretaceous-early Eocene mass extinctions in the deep sea. Geological Society of
891 America Special Publication, 247, 481- 495

892 Toon, O. B., Zahnle, K., Morrison, D., Turco, R. P., & Covey, C. (1997). Environmental perturbations
893 caused by the impacts of asteroids and comets. Reviews of Geophysics, 35(1), 41-78.

894 Verity, P. G., Brussaard, C. P., Nejstgaard, J. C., van Leeuwe, M. A., Lancelot, C., & Medlin, L. K.
895 (2007). Current understanding of Phaeocystis ecology and biogeochemistry, and perspectives for
896 future research. *Biogeochemistry*, *83*(1), 311-330.

897 Wade, B. S., Pearson, P. N., Berggren, W. A., & Pälike, H. (2011). Review and revision of Cenozoic
898 tropical planktonic foraminiferal biostratigraphy and calibration to the geomagnetic polarity and
899 astronomical time scale. Earth-Science Reviews, 104(1-3), 111-142.

900 Worzel, J. L., Bryant, W., et al, 1973, Initial Reports of the Deep Sea Drilling Project, Volume X,
901 Washington (U.S. Government Printing Office) doi:10.2973/dsdp.proc.10.1973

902 Zachos, J. C., & Arthur, M. A. (1986). Paleoceanography of the Cretaceous/Tertiary boundary event:
903 inferences from stable isotopic and other data. Paleoceanography, 1(1), 5-26.

904 Zachos, J. C., Arthur, M. A., & Dean, W. E. (1989). Geochemical evidence for suppression of pelagic
905 marine productivity at the Cretaceous/Tertiary boundary. Nature, 337(6202), 61-64.

906